XII. PLASMA MAGNETOHYDRODYNAMICS AND ENERGY CONVERSION*

Prof. E. N. Carabateas
Prof. J. A. Fay
Prof. S. I. Freedman
Prof. G. N. Hatsopoulos
Prof. W. D. Jackson
Prof. H. P. Meissner
Prof. P. L. Penfield, Jr.
Prof. D. C. Pridmore-Brown
Prof. A. H. Shapiro
Prof. J. L. Smith, Jr.
Prof. H. H. Woodson
J. L. Coggins
R. S. Cooper
F. W. Fraim III
N. Gothard
C. W. Haldeman
H. M. Heggestad
W. H. Heiser
J. B. Heywood
E. D. Hoag
P. G. Katona
F. D. Ketterer
G. B. Kliman
P. Klimowski
A. G. F. Kniazzeh
M. F. Koskinen
W. H. Levison
A. T. Lewis
J. R. Melcher
H. D. Meyer
W. T. Norris
E. S. Pierson
J. W. Poduska
D. H. Pruslin
A. R. Reti
A. Shavit
J. H. Sununu
R. G. Vanderweil
E. F. Wahl III
G. L. Wilson

A. AN ELECTROHYDRODYNAMIC AMPLIFIER

1. The Planar Amplifier

An electric field applied perpendicular to a plane conducting interface of a static fluid can produce an instability.[1] As a direct consequence of the static condition of the unperturbed interface, the instability is nonconvective.[2] If the fluid is in motion with a constant velocity V_o, there is a velocity that is such that the instability manifests itself in a convective form.

This report is concerned with investigating the dynamics of a plane jet of fluid stressed perpendicularly by an electric field, as shown in Fig. XII-1.

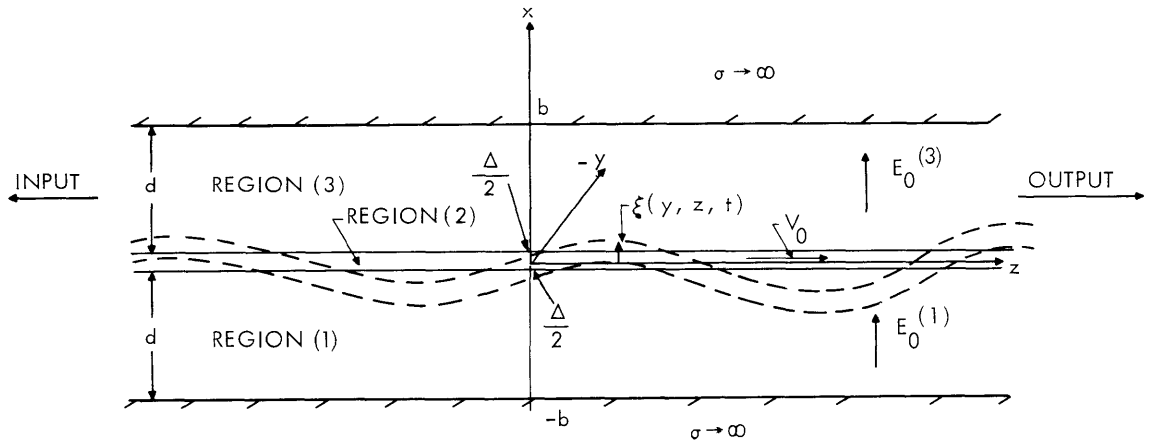

Fig. XII-1. Configuration of planar amplifying section.

*This work was supported in part by the National Science Foundation under Grant G-9330, and in part by the U.S. Air Force (Aeronautical Systems Division) under Contract AF33(616)-7624 with the Aeronautical Accessories Laboratory, Wright-Patterson Air Force Base, Ohio.

Our objective is to show the conditions for which this configuration can be made to give traveling-wave amplification of a signal that is impressed on the jet. In this case there would be a signal coupled to the flow on the upstream (input) end of the device and an output coupling at the downstream end. In the region between, the energy of the impressed ac signal would grow at the expense of the kinetic-flow energy.

The interaction considered is superficial in nature. If there is to be a significant interchange of kinetic-flow energy and ac energy stored in the electric field, the jet must offer a high surface-to-volume ratio. The planar configuration chosen here offers this advantage and is also easily tractable.

The static electric field is impressed by means of parallel plates of high conductivity (equipotentials) as shown in Fig. XII-1. These are at a distance b from the center of the jet, but may be of the same or opposite polarity, that is, $E_o^{(3)} = -|E_o^{(1)}|$ or $E_o^{(3)} = |E_o^{(1)}|$. It will be shown that the dynamics of these possibilities will be the same whether the jet supports net charge or is neutral.

a. Equations of Motion

It will be assumed that the jet moves with a uniform velocity V_o in the y direction, and that the density of the jet is sufficiently high to warrant ignoring the density of the surrounding static fluid. The fluid is taken to be inviscid and incompressible. The electrostatic equations will be sufficient to describe the electrodynamics. Hence the bulk equations are:

$$\rho\left[\frac{\partial \bar{v}}{\partial t} + (\bar{v}\cdot\nabla)\bar{v}\right] + \nabla p' = 0 \tag{1}$$

$$\nabla \cdot \bar{v} = 0 \tag{2}$$

$$\nabla \cdot \epsilon_o \bar{E} = q \tag{3}$$

$$\nabla \times \bar{E} = 0 \tag{4}$$

where $\bar{v}$ and p' are the fluid velocity and pressure; $\bar{E}$ and q are the electric field intensity and free charge density; the permittivity is ϵ_o because there is no polarization involved; and the electric field is excluded from the interior of the jet.

b. Solutions

Small perturbations of the flow are considered so that $(\bar{v}\cdot\nabla)\bar{v} \rightarrow V_o \frac{\partial \bar{v}}{\partial z}$, $\bar{E} = [E_o + e_x]\bar{a}_x + e_y\bar{a}_y + e_z\bar{a}_z$, $p' = p_o + p$. Because the bulk equations are not coupled, solutions may be written directly. If these solutions are of the form $p = p\exp(\alpha t + \beta_y y + \beta_z z)$, then

$$\begin{bmatrix} \hat{p} \\ \hat{e}_z \end{bmatrix} = \begin{bmatrix} A_1 \\ C_1 \end{bmatrix} e^{kx} + \begin{bmatrix} A_2 \\ C_2 \end{bmatrix} e^{-kx}; \quad k^2 = -\beta_y^2 - \beta_z^2; \quad \omega^2 = -a^2, \tag{5}$$

where

$$\hat{v}_x = \frac{-k}{\rho(a+\beta_z V_o)} \left[A_1 e^{kx} - A_2 e^{-kx} \right] \tag{6}$$

$$\hat{v}_y = \frac{-\beta_y}{\rho(a+\beta_z V_o)} \left[A_1 e^{kx} - A_2 e^{-kx} \right] \tag{7}$$

$$\hat{v}_z = \frac{-\beta_z}{\rho(a+\beta_z V_o)} \left[A_1 e^{kx} + A_2 e^{-kx} \right] \tag{8}$$

$$\hat{e}_x = \frac{k}{\beta_z} \left[C_1 e^{kx} - C_2 e^{-kx} \right] \tag{9}$$

$$\hat{e}_y = \frac{\beta_y}{\beta_z} \left[C_1 e^{kx} + C_2 e^{-kx} \right] \tag{10}$$

The surfaces are defined by the conditions

$$\hat{\xi}(a+\beta_z V_o) - \hat{v}_x \Big|_{x = \pm \frac{\Delta}{2}} = 0, \tag{11}$$

and

$$\bar{n} = -\bar{a}_y \beta_y \hat{\xi} - \bar{a}_z \beta_z \hat{\xi}, \tag{12}$$

where $\bar{a}_y$ and $\bar{a}_z$ are unit normals in the directions of the axes, and n is a unit normal vector perpendicular to the interfaces. (The unit normal is directed in the positive x direction for both interfaces.)

As a result of the negligible mass density in regions exterior to the jet, the boundary conditions on the normal velocities at the interfaces are satisfied identically. The remaining conditions, resulting from integrating Eqs. 1, 3, and 4 across the interfaces, determine the A's and C's.

$$\left\{ n_a \left(\begin{bmatrix} -p' \\ p' \end{bmatrix} + k^2 T \hat{\xi} \right) - \frac{\sigma_f}{2} \begin{bmatrix} E_a^{(3)} \\ E_a^{(1)} \end{bmatrix} \right\}_{x = \pm \frac{\Delta}{2}} = 0, \tag{13}$$

where the surface charge densities are

$$\sigma_f\Big|_{x=\pm\frac{\Delta}{2}} = \epsilon_o \bar{n} \cdot \left[\begin{matrix}\bar{E}^{(3)} \\ \bar{E}^{(1)}\end{matrix}\right]_{x=\pm\frac{\Delta}{2}} \tag{14}$$

$$\bar{n} \times \left[\begin{matrix}\bar{E}^{(3)} \\ -\bar{E}^{(1)}\end{matrix}\right]_{x=\pm\frac{\Delta}{2}} = 0 \tag{15}$$

The pressure has been defined as zero in regions (1) and (3). At the exterior boundaries (x=±b)

$$\bar{n} \times \bar{E} = 0. \tag{16}$$

Six of the conditions given by Eqs. 13-16 are independent, the first components of Eq. 13 and the second of Eqs. 15 and 16.

$$\left\{\left[\begin{matrix}-\hat{p} \\ \hat{p}\end{matrix}\right] + \frac{\hat{v}_x k^2 T}{(a+\beta_z V_o)} + \left[\begin{matrix}-\epsilon_o E_o^{(3)} e_x^{(3)} \\ \epsilon_o E_o^{(1)} e_x^{(1)}\end{matrix}\right]\right\}_{x=\pm\frac{\Delta}{2}} = 0 \tag{17}$$

$$\left\{\frac{\beta_z \hat{v}_x}{(a+\beta_z V_o)}\left[\begin{matrix}E_o^{(3)} \\ E_o^{(1)}\end{matrix}\right] + \left[\begin{matrix}e_z^{(3)} \\ e_z^{(1)}\end{matrix}\right]\right\}_{x=\pm\frac{\Delta}{2}} = 0 \tag{18}$$

$$\left\{\begin{matrix}e_z^{(3)} \\ e_z^{(1)}\end{matrix}\right\}_{x=\pm b} = 0. \tag{19}$$

If the solutions, Eqs. 5-10, are now used to evaluate the boundary conditions of Eqs. 17-19, six homogeneous equations for the coefficients $A_1^{(2)}$, $A_2^{(2)}$, $C_1^{(3)}$, $C_2^{(3)}$, $C_1^{(1)}$, $C_2^{(1)}$ are obtained. The compatibility condition on these equations is the required dispersion relation.

c. Dispersion Relation

The dispersion equation can be written in the form

$$\rho(a+\beta_z V_o)^2 = k^2\left[E_o^2 \epsilon_o \coth(kd) - kT\right]\psi^{\pm}. \tag{20}$$

There are two modes in which a given wavelength perturbation may occur. These

correspond to two functional relations for $\psi^{\pm}$:

$$\psi^{\pm} = \coth(k\Delta) \pm \sqrt{\coth^2(k\Delta) - 1}.$$

Note that the identity of these modes depends only on the ratio of the perturbation wavelength to the jet thickness. If this ratio is small ($\Delta k \gg 1$), both modes have the same eigenvalues, that is, $\psi^+ \to \psi^- \to 1$. In this limit of short-wavelength waves, the interfaces of the jet are uncorrelated in their motion. The dispersion equation is the same as that which would be obtained if only one interface were considered and the other interface were at infinity.

On the other hand, if the thickness Δ is made small enough that all wavelengths are long compared with the thickness ($\Delta k \ll 1$), then $\psi^- \to 0$ and $\psi^+ \to \frac{2}{\Delta k}$. Under this condition, the interfaces interact strongly so as to limit the modes to those corresponding to ψ^+. Equations 17-19 show that in this limit the interfaces move in phase. (The velocities are in phase as shown in Fig. XII-1. In circular geometry this would be called a "kinked" mode.)

A practical device would require a high surface-to-volume ratio. For this reason, modes corresponding to ψ^+ in the limit in which $\Delta k \ll 1$ will be considered here. Hence the relation between frequency and wave number is given by

$$(\omega + k_z V_o)^2 = \left[k^2 V_k^2 - 2k\omega_k V_k \coth kd\right], \tag{21}$$

where

$$V_k = \sqrt{\frac{2T}{\Delta\rho}}$$

$$\omega_k V_k = \frac{E_o^2 \epsilon_o}{\Delta\rho}.$$

The argument (kd) in this expression is an index to the degree of interaction between the jet and individual charges on the electrodes. If $kd \gg 1$, then the charges on the plates interact with those on the surfaces of the jet in a collective way. Conversely, if $kd \ll 1$, then charges on the jet strongly "feel" their images on the plates. Clearly, this last condition is desirable in an exciter section in which the jet would be driven by space periodic variations in the plate bias. In the amplification section, shown in Fig. XII-1, the essential gain characteristics of the device are altered by changing kd, but this section may be operated in either regime or somewhere in between. These limits will be considered separately.

The convective or nonconvective nature of the instability is independent of the value of kd, as may be seen by viewing the plot of Eq. 21 (Fig. XII-2) in the complex ω plane for real values of k.[2] (The assumption will be made in the following discussion that

there is no y-dependence of the waves considered, that is, $k = k_z$.)

It is clear that a necessary condition for a convective instability is that $V_o > V_k$, where V_k is the phase velocity of a capillary wave on a stationary layer of fluid of thickness Δ (see Eq. 21). Equation 21 is easily solved for k in the limit of strong and weak interactions with the external plates ($kd \ll 1$, $kd \gg 1$). The complex k plots for real ω for these two limits are shown in Fig. XII-3.

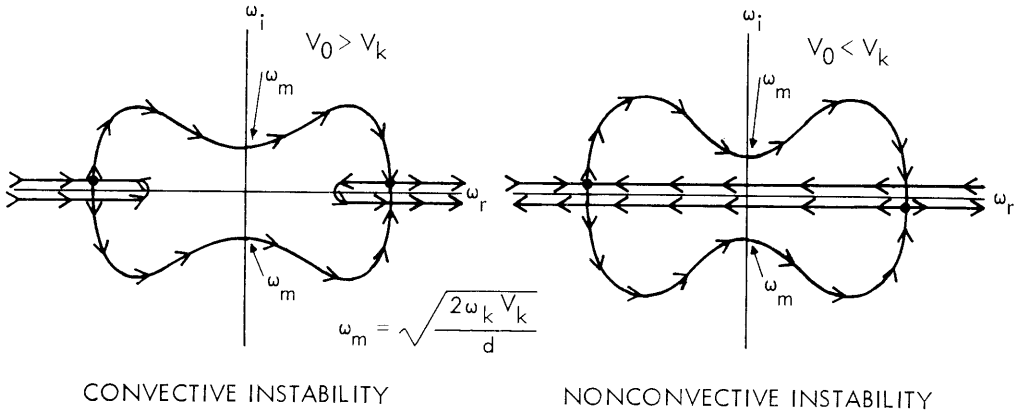

Fig. XII-2. Complex-frequency plot for real wave number. Arrows indicate the direction of increasing k.

The peak gain with the plates close to the jet comes at zero frequency. With the plates removed so that $kd \gg 1$, the peak gain corresponds to

$$k_i = \pm \frac{\omega_k}{\sqrt{\left(V_o^2 - V_k^2\right)}} \tag{22}$$

with

$$\omega = \frac{1}{2}\omega_b = \frac{\omega_k}{2}\left[\frac{V_o}{V_k} + \sqrt{\frac{V_o^2}{V_k^2} - 1}\right].$$

Note that in the limit of $kd \gg 1$, the cutoff frequency, and the frequency for maximum gain and peak k_i vary linearly with ω_k (for example, the bias voltage squared). On the other hand, the variation of these parameters is proportional to $\sqrt{\omega_k}$ if $kd \ll 1$. If $V_o \gg V_k$, the cutoff frequency is closely approximated by ω_a in Fig. XII-3. A dimensionless plot of this frequency as a function of applied

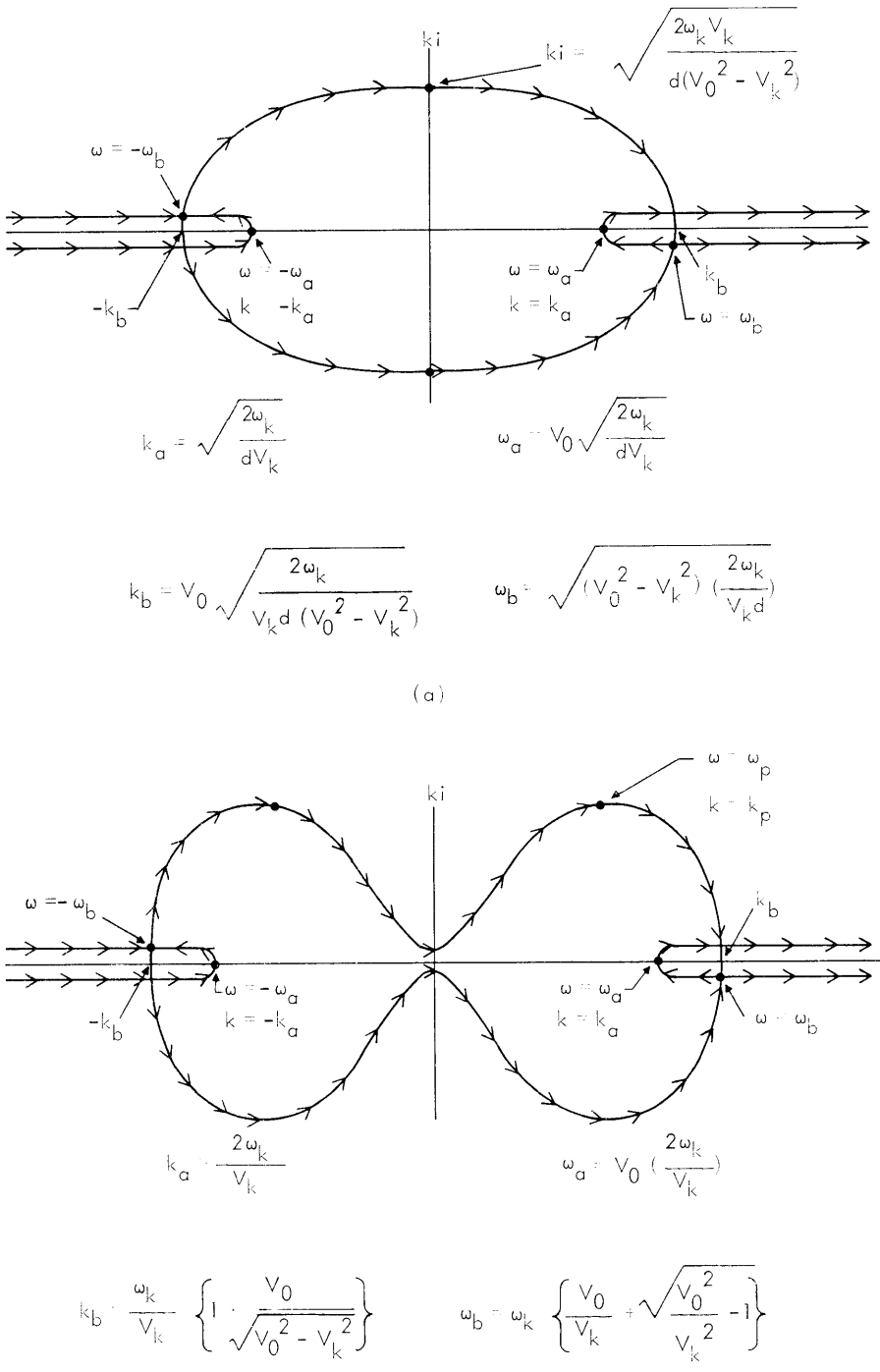

Fig. XII-3. Complex k plots for real ω. (a) Strong plate coupling ($kd \ll 1$). (b) Weak plate coupling ($kd \gg 1$).

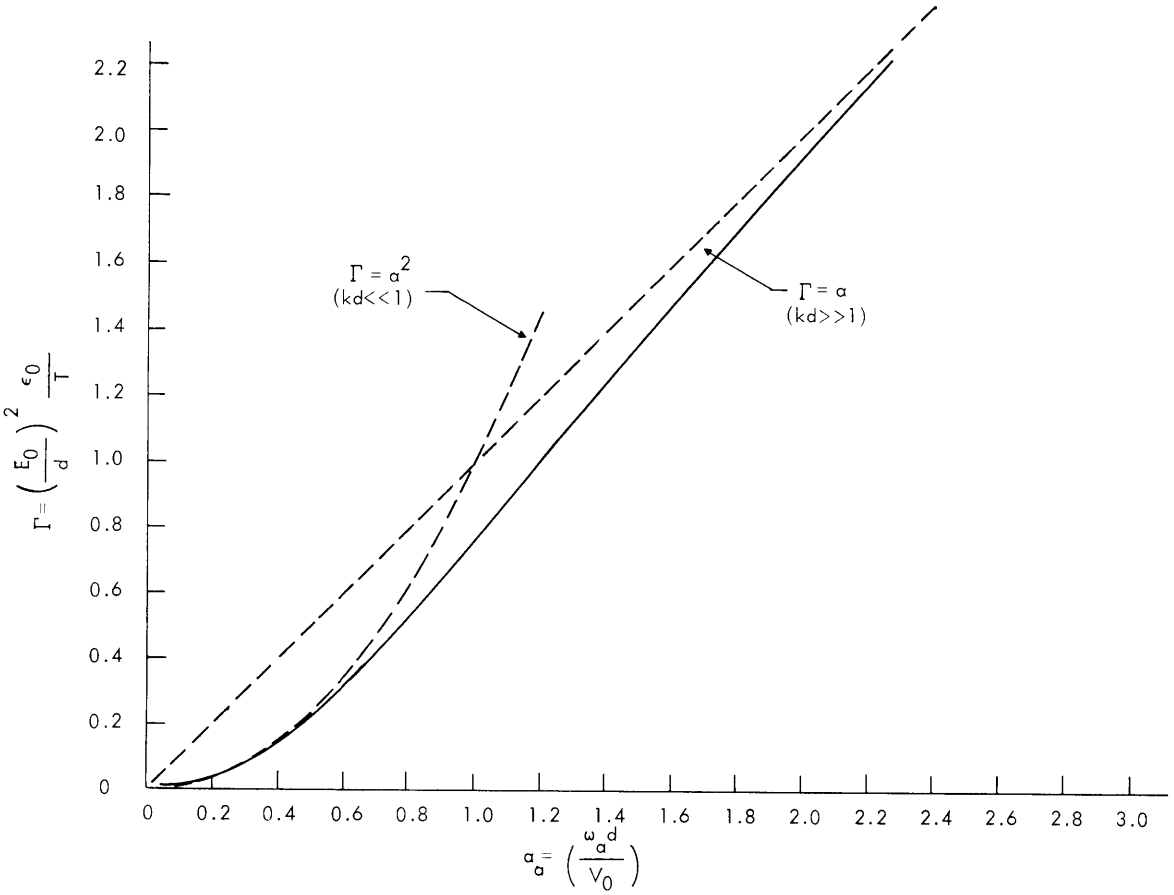

Fig. XII-4. Cutoff frequency ω_c as a function of Γ for $V_o \gg V_k$.

voltage for $V_o \gg V_k$ is given in Fig. XII-4. The transition from the regime kd » 1 to the regime where kd « 1 may be seen to take place in the region where kd = 1.

2. The Circular Amplifier

Although the planar jet can provide a high surface-to-volume ratio, as well as serve as a simple example of the dynamics of a convective instability, it does not admit of experimental investigation as easily as does the circular jet. It is now our purpose to describe briefly the theoretical dynamics involved when a circular conducting convecting jet is stressed by a radial electric field, and to describe correlative experiments that have been performed.

An ordinary jet of water (not stressed by electric fields) was used as a traveling-wave amplifier as early as 1890.[3] However, the dynamics involved were not considered in a modern context until recently.[4] In this amplifier, advantage was taken of the natural

capillary instability of a circular jet to achieve a purely mechanical interchange of steady flow energy and periodic perturbations of the jet.

The stability of an electrified jet of liquid was of interest to investigators before the turn of the century. It was observed that the capillary instability could be arrested to a certain extent by inducing charges on the surface of the jet.[3] A theoretical investigation that explained this observation in principle was given by Basset,[5] in 1894. Other previous discussions of charges induced on capillary interfaces[6] are also confined to questions of nonconvective instability.

a. Problem Description

The configuration considered here is the circular analog of the planar jet. (See Fig. XII-5.) A circular conducting jet of radius R moves with an unperturbed velocity

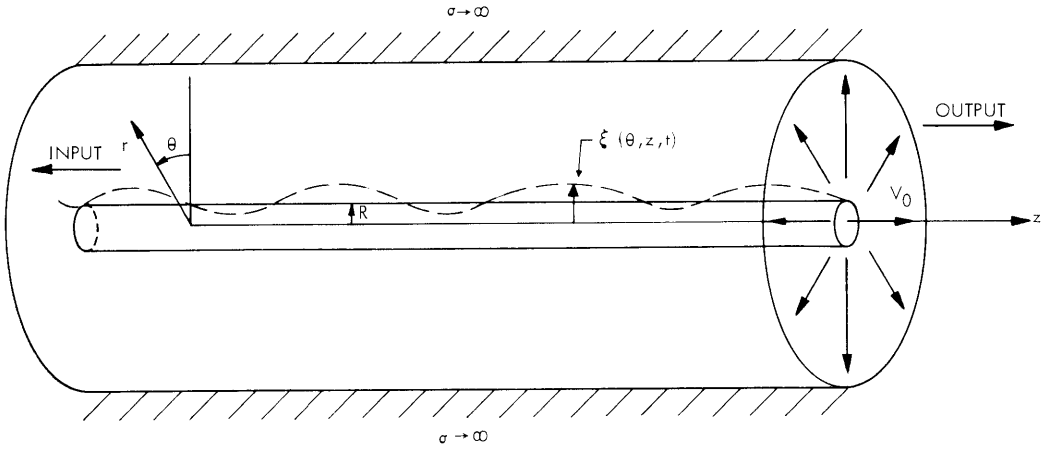

Fig. XII-5. Configuration of amplifying section for cylindrical jet.

V_o along the z axis. A radial electric field stresses the jet and terminates on a highly conducting cylinder of radius b. Hence the unperturbed electric field has the form $\overline{E} = V/r$ when V = (potential difference)/$\ln \frac{b}{R}$.

The analysis of this problem is similar to that described above and will not be given in detail here. The only essential difference arises from the radial dependence of the unperturbed electric field, a circumstance that results in a perturbation at the surface that is experiencing an electric field that depends directly on the perturbation itself.

b. Dispersion Relation

If solutions of the form $p = \hat{p} \exp[j(\omega t+m\theta-kz)]$ are assumed, the dispersion equation given by Eq. 23 results.

$$(\omega - kV_o)^2 = \frac{T}{\rho R^3}\left[\frac{1}{K_m(kR)}\right]\left\{\Gamma(1+S_m(kR, kb))-(1-m^2)+(kR)^2\right\} \tag{23}$$

where

$$K_m(kR) = \frac{J_m(jkR)}{(jkR)\, J'_m(jkR)}$$

$$S_m(kR, kb) = jkR\left[\frac{H'_m(jkR)\, J_m(jkb) - H_m(jkb)\, J'_m(jkR)}{H_m(jkR)\, J_m(jkb) - J_m(jkR)\, H_m(jkb)}\right]$$

$$\Gamma = \frac{V^2 \epsilon_o}{RT}.$$

Equation 23 is the circular analog of Eq. 20. However, the effect of varying the jet radius and the radius of the conducting wall can be accounted for by Bessel and Hankel

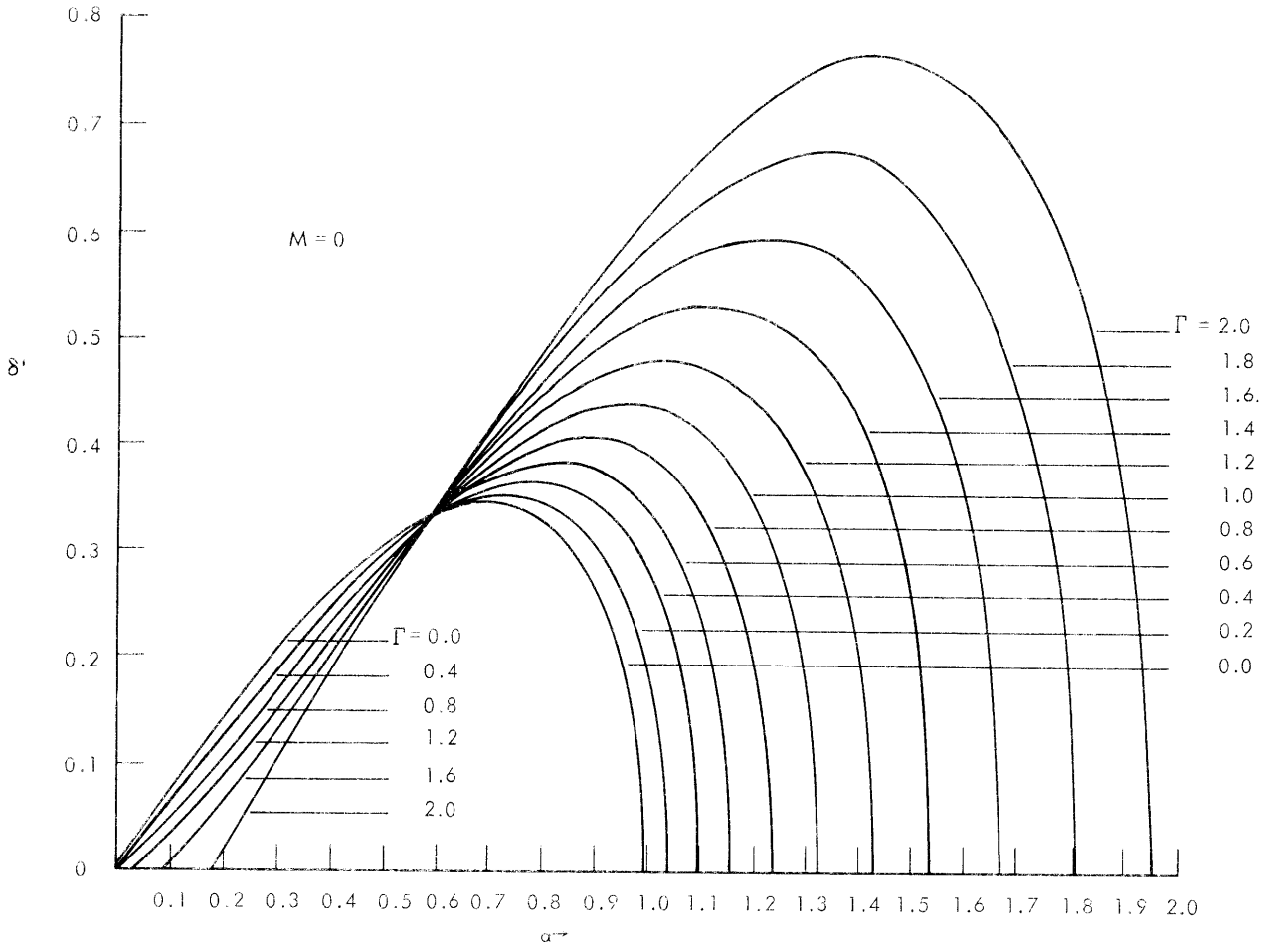

Fig. XII-6. Circular jet gain as a function of normalized frequency in the m = 0 mode.

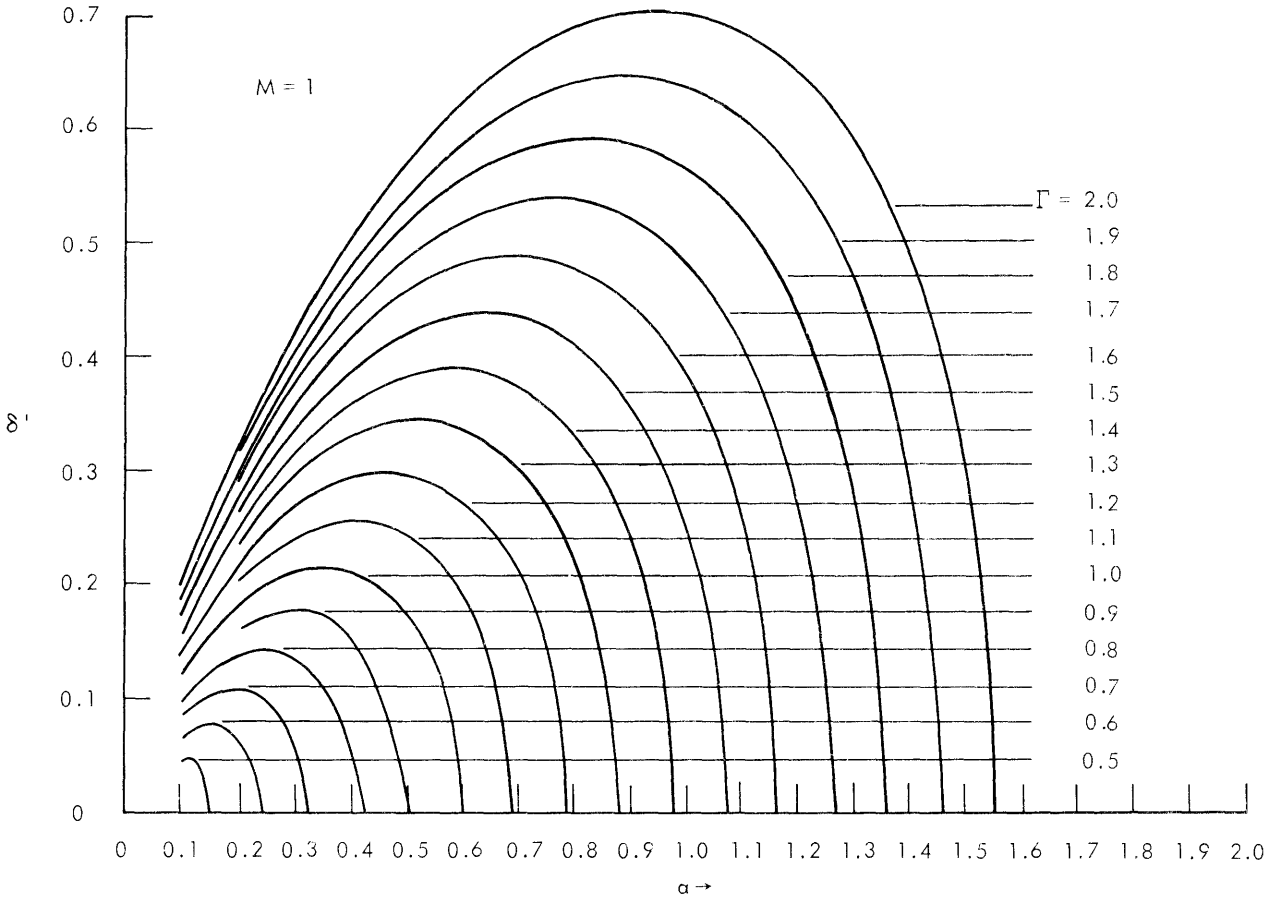

Fig. XII-7. Circular jet gain as a function of normalized frequency in the m = 1 mode.

functions of the first kind and imaginary argument. (For k with a negative real part the Hankel function of the second kind must be used.) However, the functions $K_m(kR)$ and $S_m(kR, kb)$ can be shown to be even. If the radius of the outer conducting cylinder is much greater than perturbation wavelengths on the jet, $(kb \gg 1)$,

$$S_m(kR, kb) \rightarrow \frac{(jkR)\, H'_m(jkR)}{H_m(jkR)}. \tag{24}$$

It is apparent that it is not convenient to find complex values of k for real values of ω, as we did before. However, if the jet velocity greatly exceeds the capillary wave velocity (this was $V_o \gg V_k$ before), a good approximation for k is $kR = \frac{\omega R}{V_o} + \delta R = a + \delta R$, where δ is imaginary for a growing wave. In this case

$$\delta' \cong \pm j \left\{ \left[\frac{1}{K_m(a)} \right] \left[(1-m^2) - (a)^2 - \Gamma \left(1 + \frac{H'_m(ja)(ja)}{H_m(ja)} \right) \right] \right\}^{1/2} \tag{25}$$

where

$$\delta' = \delta\sqrt{\frac{R^3\rho V_o^2}{T}} .$$

The function $K_m(a)$ is positive for real arguments. If there is no electric field applied (Γ=0), Eq. 25 shows that if m = 0, there may still be gain. This is the mode of the mechanical traveling-wave amplifier mentioned above.

The behavior of δ' as a function of frequency is shown in Figs. XII-6 and XII-7. Note that for $a < 0.58$ and m = 0 the gain is decreased by increasing the electric field. This is the stabilization effect mentioned earlier. The remaining modes have no $\Gamma = 0$ gain. In a way similar to that for the planar jet, the frequencies for peak and cutoff gain are increased by increasing the electric field. For values of $\Gamma > 1$, the m = 0 mode has a lower cutoff frequency, as well as an upper one.

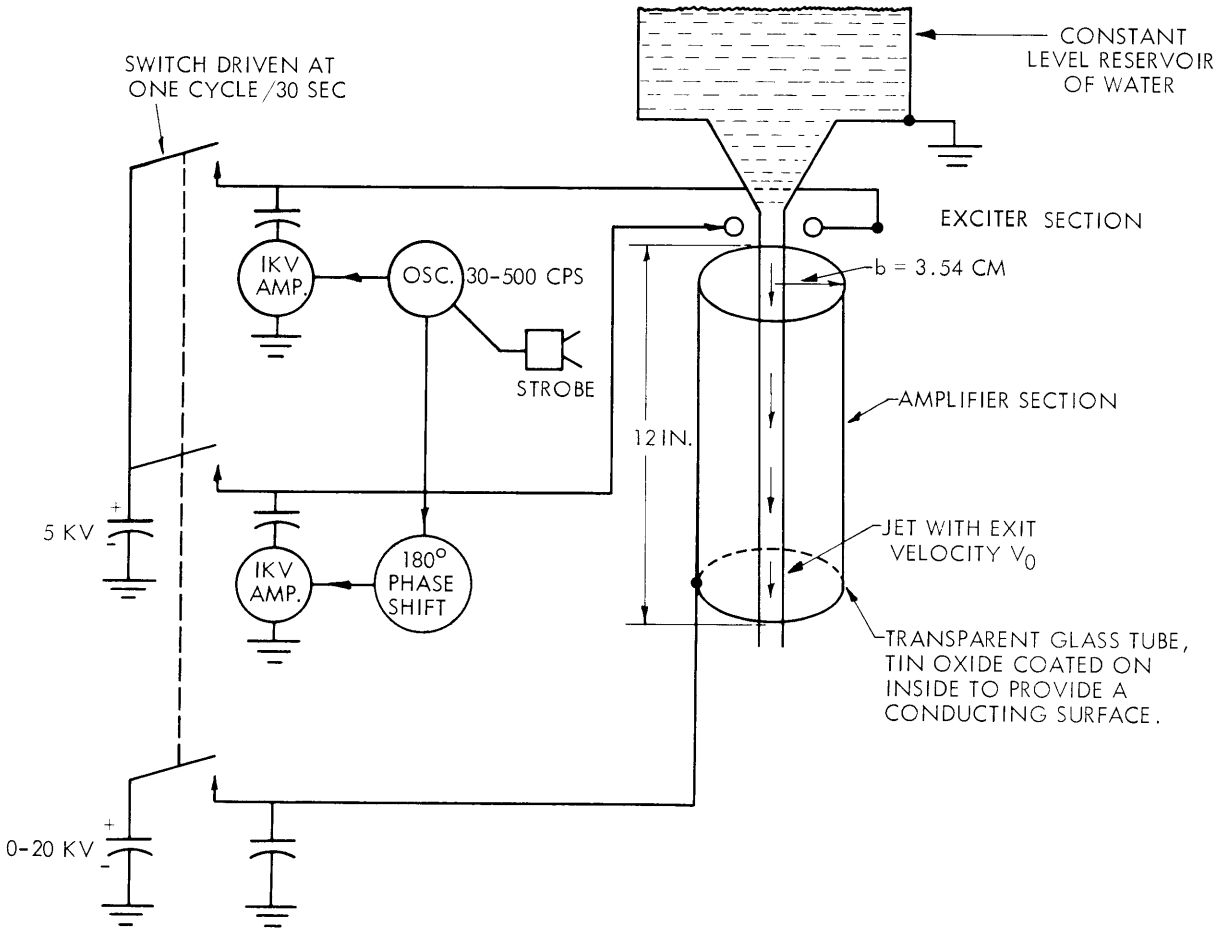

Fig. XII-8. Circular jet experiment (m=1).

c. Experiment

One of the virtues of electrohydrodynamics is the physical reality of simple idealized models such as those used in the previous sections. Water is a "highly" conducting fluid and can be used to illustrate the validity of the model. An experiment is considered here that shows the physical nature of the circular m = 1 mode. The experimental apparatus is shown in Fig. XII-8. A jet of water is projected along the axis of a conducting glass cylinder. This cylinder is biased with respect to the jet to voltages in the range 0-20 kv. Just before the jet enters this amplifier section, an ac signal is impressed on the jet surface by means of two electrodes located on opposite sides of the jet. These electrodes support an ac voltage of approximately 1 kv p-p, 180° out of phase. The ac voltage is superimposed on a 5-kv dc bias. It is important that these electrodes be placed close to the jet ($kb \ll 1$) for the interaction to be strong.

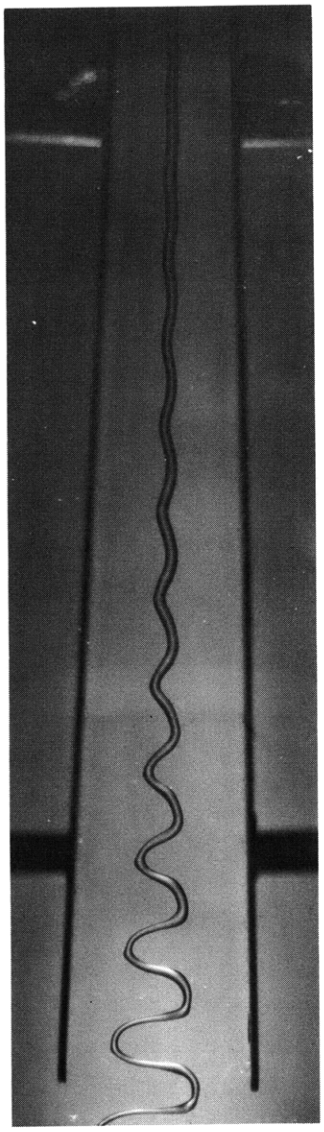

Fig. XII-9. Jet passing through the amplifier section.

The dc bias on all electrodes was switched on and off, and the voltages were maintained during the off periods by capacitors. This provided an operating period during the off periods when the system was free from 60-cycle ripple from the power supplies.

A picture of the jet passing through the amplifier section is shown in Fig. XII-9. (For this picture the glass tube was replaced by diverging parallel plates to increase the visibility and decrease the rate of amplification.)

As shown in Fig. XII-9, the jet is moving downward at approximately 4.5 m/sec and each undulation is reversing its phase 250 times per second. The length of the jet is approximately 10 inches. It is important to note that although this picture was taken instantaneously, it characterizes the steady-state appearance of the jet as viewed under the light of a strobotac synchronized with the driving frequency.

In general, it is found that the gain first increases and then cuts off as the frequency

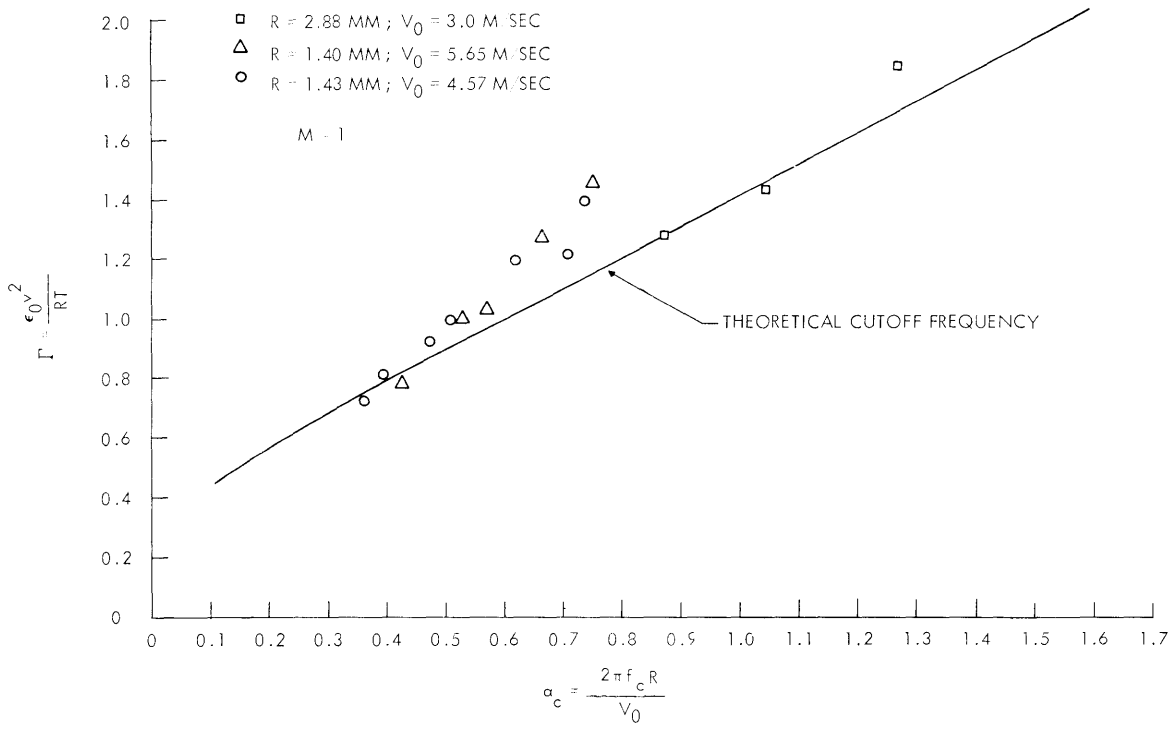

Fig. XII-10. Experimental cutoff frequency as a function of Γ for m = 1.

is increased, in accordance with the behavior of the gain curves of Fig. XII-7. Moreover, the gain and cutoff frequency of the device do increase with increasing voltage.

The cutoff frequency was measured and the corresponding conditions converted to the dimensionless numbers α and Γ. These data, together with the theoretical prediction, are shown in Fig. XII-10. Three different jet diameters and velocities were used. The correlation suggests that the theoretical model is meaningful. This is especially true when the errors involved in making the plot of Fig. XII-10 are recognized. The flow velocity V_0 and jet radius R do not remain constant as the jet accelerates through the amplifier section. In measuring the cutoff frequency, it is reasonable to use the least value of R because this results in the highest cutoff frequency. This was the procedure used here, with R and V_0 measured at the amplifier exit. However, the normalized frequency α_c of Fig. XII-10 is then proportional to the cube of R, so that small errors in R strongly influence the data.

The range of frequencies over which cutoff measurements can be made is limited at low and high frequencies (see Fig. XII-10). At very low cutoff frequencies (low Γ) the gain in the exciter section is sufficient to obscure the cutoff point. At high cutoff frequencies (high Γ) it is difficult to maintain mode identity, as would be expected from a comparison of Figs. XII-6 and XII-7.

J. R. Melcher

References

1. J. R. Melcher, Electrohydrodynamic and magnetohydrodynamic surface waves and instabilities, Phys. Fluids 4, 11 (1961).

2. P. A. Sturrock, Kinematics of growing waves, Phys. Rev. 112, 1438 (1958).

3. C. V. Boys, Soap Bubbles (Dover Publications, Inc., New York, 1959), p. 84.

4. J. R. Pierce, An interesting wave amplifier, Trans. IRE, Vol. ED-1, p. 73 (1960).

5. A. B. Basset, Waves and jets in a viscous liquid, Am. J. Math. 16, 93 (1894).

6. J. W. S. Rayleigh, The Theory of Sound (Dover Publications, Inc., New York, 1945), Vol. II, p. 374.

B. TRAVELING SPACE-CHARGE WAVES IN D-C DISCHARGES. I.

1. Introduction

My purpose in this report is to outline the results of an analysis of some spontaneously generated oscillations that occur in the positive column of dc discharge tubes. The oscillations were found to be traveling space-charge waves accompanied by a region of intense excitation within the gas. These waves have long been observed by spectroscopists and gas-discharge physicists and classically are called "moving striations." Also, a diffusion model for the plasma is described and equations describing the time- and space-dependent diffusive particle flow for the assumed model are derived. The solutions to these equations and their relation to the experimental observations are being considered at the present time.

2. Description of Experiments

Observations of moving striations were carried out in a cylindrical discharge tube, 60 cm in length and 5 cm in diameter. The two plane, circular molybdenum electrodes were both movable. The cathode and anode were 2 cm and 1 cm in diameter, respectively, and the electrode-supporting structure behind each electrode was carefully shielded from the discharge region by mica shields attached to the movable electrodes.

Two fixed Langmuir probes were located 30 cm from the end of the tube. They could be moved radially and, since the electrodes could be moved axially, the probes had access to every region of the interelectrode space.

The range of pressures in which striations have been observed in these studies includes the region from approximately 1-30 mm Hg. They have been observed in all of the gases studied: argon, helium, hydrogen, nitrogen, and air; and, in fact, for most operating conditions, they are more likely to be present than not. It is clear that any

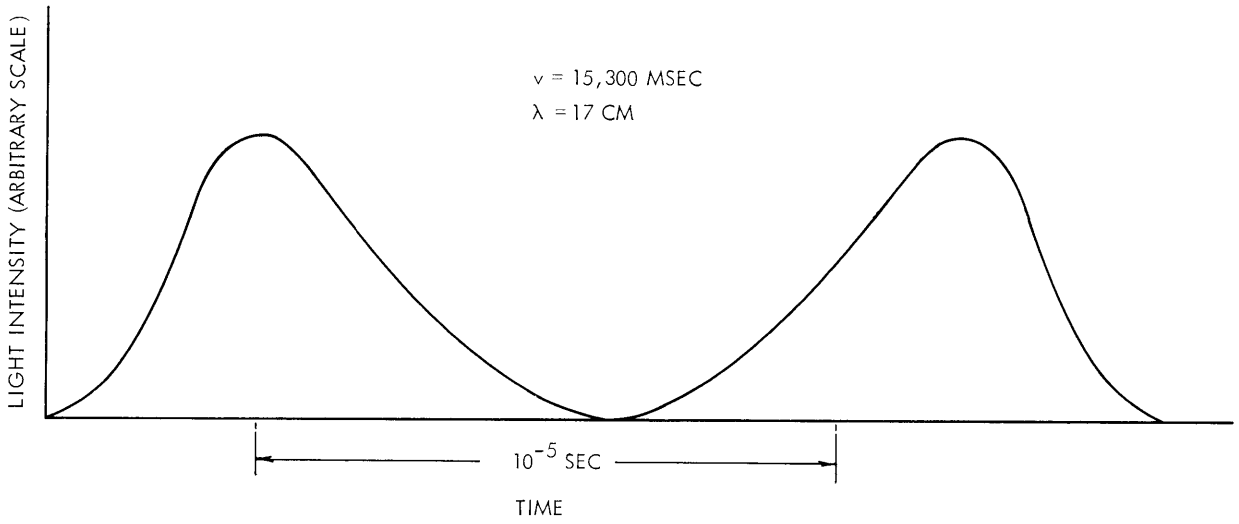

Fig. XII-11. Light intensity vs time, typical in argon at 3 mm Hg.

theory of the positive column which does not include these waves is incomplete, for they rank as one of the major characteristics of the discharge.

The shape of the light pulse, which typically travels toward the anode, is shown in Fig. XII-11. The observations upon which this figure is based were made by displaying the output of a 931A phototube on an oscilloscope. Under extreme conditions, the leading edge of the wave can become very steep; and, instead of the te^{-t} appearance, the wave assumes almost a saw-tooth form. Note that the light intensity goes to zero between successive intensity maxima. There are also examples for which the intensity variation is nearly a sinusoidal ripple of less than 10 per cent, which is superimposed upon a steady background illumination.

By synchronizing the oscilloscope with a second, fixed phototube, the direction and speed of travel may be measured by moving the scanning phototube axially. In general, the waves arise in the glow at the cathode end of the positive column, increase rapidly in amplitude, and move simultaneously toward the anode. The light intensity saturates after approximately 1 cm of travel and remains at relatively constant amplitude during the rest of the journey to the anode. Occasionally, the light intensity is modulated 10-20 per cent every half-wavelength as the wave progresses. Faint standing striations can sometimes be seen at the points of maximum intensity when this modulation is present.

Velocities range from tens to thousands of meters per second, and frequencies range from 500 cps to 1 mc, the range depending on the type of gas, the pressure, and the current. In simple cylindrical tubes sustaining cold-cathode glow discharges between plane electrodes, the frequency can be exceedingly stable, and the oscillations will continue indefinitely unabated. Wavelengths range from one-thirtieth of the electrode separation up to approximately the length of the positive column.

Changing the tube current or the gas pressure generally causes smooth changes in the frequency and wavelength of the moving disturbance. At certain critical values of current and pressure, however, the frequency may jump discontinuously to nearly an integral multiple or submultiple of the original frequency. At some values of these parameters there may be more than one stable operating frequency that depends on the manner in which the point of operation is approached. Often the operation is very unstable, and the mode of operation appears to be jumping randomly from one "stable" mode to the other.

Changing the cathode structure to cylindrical, cubical or other nonplanar shapes will interfere markedly with the periodicity of the waves. This interference has not been pointed out previously and tends to give the impression that traveling striations never appear as strictly periodic phenomena. This factor also makes their study much more difficult in tubes with other than simple geometries. Others have employed heated cathodes and have observed striations. It is unlikely, therefore, that the nature of the cathode surface plays any major role in the propagation phenomenon, although it may well influence the initiation of the wave.

Numerous probe measurements have revealed that the electric field intensity and the electron density rise very rapidly to two or three times their average values in the

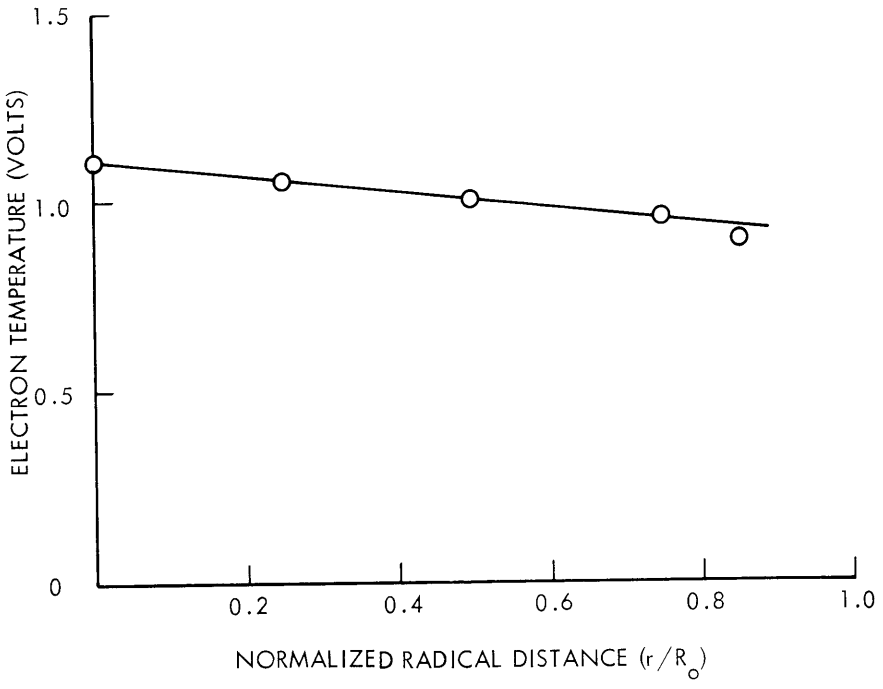

Fig. XII-12. Electron temperature vs normalized radial distance in argon at 3 mm Hg.

region of the wave front. The electron temperature also rises very slightly at the wave front. These results confirm those of Pupp.[1] In addition, radial measurements show that the electron temperature varies little across the tube from the central value (Fig. XII-12). A reasonable picture of the wave begins to emerge in the form of a potential discontinuity traveling up the background potential gradient, exciting background gas atoms through electron acceleration, and manifesting a non-negligible separation of the positive and negative charges in the plasma.

The voltage and current of the electrodes of the discharge tube may be affected severely upon the arrival of the wave front at the anode. Typically, the voltage across the tube is depressed, and the current rises 1-5 per cent if neither are constrained by the source.

External circuit constraints do not alter the waveform, velocity or frequency of the propagating wave more than 1 per cent in all cases examined. For instance, although 20 μf of capacitance shunting the tube decreases the voltage fluctuation from approximately 2 volts to 10 mv, the current fluctuation remains unchanged; the frequency and velocity are unchanged; and the waveform is only slightly affected. Dual results are obtained when a tuned, parallel resonant circuit is introduced to block the fundamental component of the current.

At any given pressure there is a particular tube current below which the waves cease to propagate. Some gases, such as nitrogen and helium, also exhibit upper cutoff limits. The upper limits have not been observed for hydrogen and argon because of power-supply limitation. This effect has not, to my knowledge, been reported previously.

When a tube is operating near the cutoff limit with no striations propagating, it is

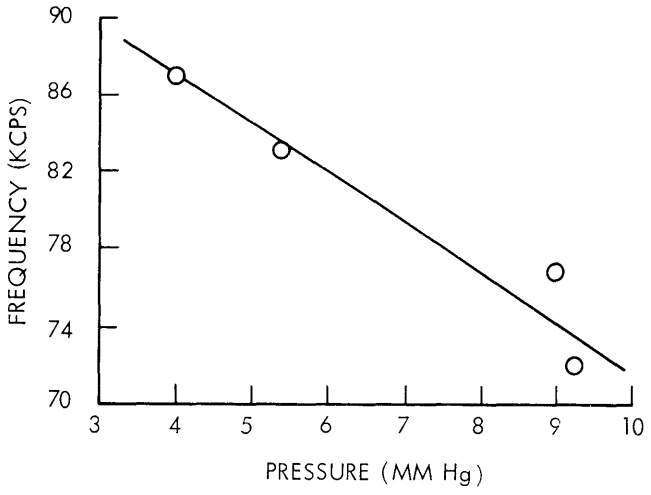

Fig. XII-13. Pressure dependence of the frequency of moving striations in argon at approximately constant electron temperature.

possible to induce striations that will propagate through the column. Three techniques have been found to accomplish this. First, a pulse change in the voltage applied to the electrodes will initiate a single striation at each pulse. Second, a pulse applied to a probe in the positive column will cause a striation to move both toward the anode and toward the cathode. The one propagating toward the cathode generally damps in a very short distance. The one moving toward the anode initially decreases in amplitude and then increases in amplitude as it enters the immediate anode vicinity. Finally, a wave may even be generated by pulsing the voltage on a ring that is external to the tube and encircling it.

There has been some speculation that moving striations are either soundlike in nature or that they induce an associated sound wave caused by the collision of heavy ions with the

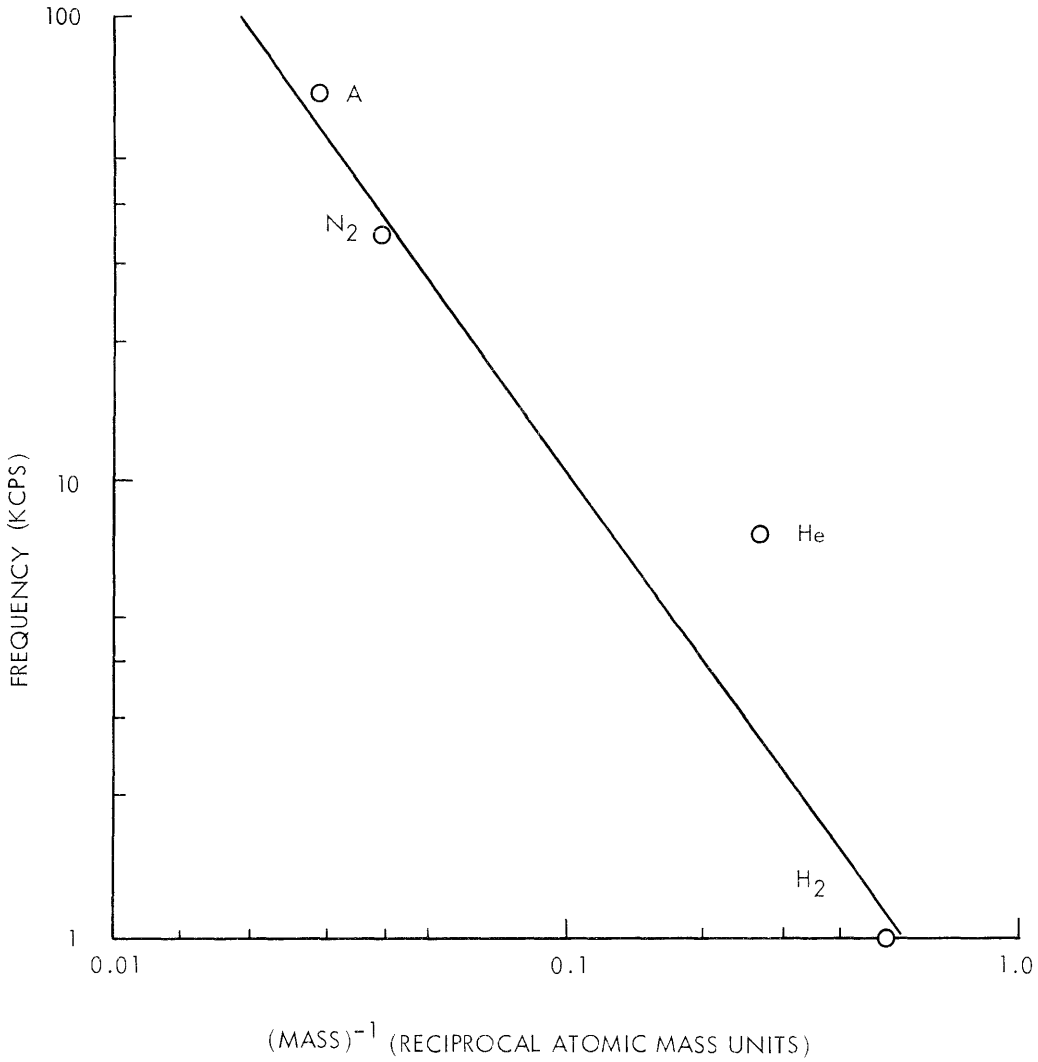

Fig. XII-14. Log-Log graph of frequency vs ionic mass for various gases.

background gas. It might be expected that an ordinary crystal microphone placed against the tube might reveal their presence. However, tests have shown that, if present, they were not detectable with the external audio system.

Langmuir[2] indicates that in the long-wave limit the ion oscillations that he describes would have a frequency dependence

$$f = \frac{1}{L}\left(\frac{kT_e}{M_i}\right)^{1/2},$$

where L is a characteristic length of the system, M_i is the mass of a gas ion, and T_e is the electron temperature. Note that f is independent of pressure.

Figure XII-13 indicates a typical variation of frequency with pressure in argon at approximately constant electron temperature. Figure XII-14 shows frequency plotted against reciprocal mass for several different gases. No attempt was made to equalize the temperatures or pressures; but the frequencies are characteristic of the gas over a wide range of these parameters and do not change by orders of magnitude. Instead of a rising curve, which would be characteristic of the ion sound-wave theory, there is a falling dependence on $1/M_i$.

These descriptions of experimental results indicate in some detail the fundamental character of the process under investigation. The next step is to attempt to construct a rational description of a plasma that will exhibit the characteristics described.

3. Theory

Most theoretical descriptions of glow discharges consider the plasma of the positive column to be a continuous fluid composed of an intermixture of electrons and ions. Therefore, the electron and ion densities are assumed to be continuous functions of position. The charged particles are assumed to be in equilibrium with one another and with the fields influencing them, so that all time variations of the variables that are of interest are ignored. The gas is also assumed to be neutral everywhere.

In all regions where the assumption of charge neutrality obviously breaks down such as in the sheaths near the walls and electrodes more precise analysis of microscopic processes can be made by applying kinetic theory to determine individual particle trajectories. Averages are taken, and the resulting functions of interest near the boundary are matched to their counterparts in the body of the plasma.

Justification for the assumption of a continuous medium is usually offered on the basis of comparison of the small collision mean-free paths of the various particles with the dimensions of the container and of the wavelengths, and so forth, of the variables of interest. In published works these assumptions have generally been stated with no detailed discussion of their validity. Actually, because the mean-free path for electrons

is a strong function of electron energy in the range of energies that are important in glow discharges, more consideration should be given to the approximations involved.

Experiments show that the plasma is not strictly in equilibrium, for there are large, time-dependent fluctuations in the variables of interest. Indeed, some mechanism of feedback causes the time variations to be periodic in most cases. Hence, the assumption that all time derivatives may be set equal to zero cannot be used to determine the nature of these fluctuations.

It is of interest to look carefully at the simple diffusion model of the positive column to determine if traveling-wave solutions are possible. In the present discussion we shall neglect the formidable arguments against using the simplified theory. However, these must be considered in detail before major success may be claimed for the theoretical method. This simplified theory can either be modified to make it suitable or will have to be abandoned for a much more complete (and hence more complex) model.

In the positive column of a dc discharge there are several different species of particles, positive and negative ions, free electrons, neutral gas atoms, and excited atoms. By far the most numerous are the neutral atoms, since the ionization percentage is always exceedingly small in this type of discharge. We shall follow, in part, the developments of Allis[3] and Stewart[4] here. In general, for any of the species the conservation of particles in a unit volume of the plasma demands that the following equation be satisfied:

$$n^{(j)}(\vec{r},t) = -\nabla \cdot \vec{J}_{(j)}(\vec{r},t) + R_i^{(j)}(\vec{r},t) - R_a^{(j)}(\vec{r},t), \tag{1}$$

where $n^{(j)}(\vec{r},t)$ is the particle density of the j^{th} species in configuration space; t is time; $J_{(j)}(\vec{r},t,\vec{E})$ is the particle current density vector for the j^{th} species; $R_i^{(j)}(\vec{r},t)$ is the rate of creation of particles per unit volume; $R_a^{(j)}(\vec{r},t)$ is the rate of annihilation of particles per unit volume, and E is the electric field intensity.

Since only the charged particles can interact with the fields, only the equations for the singly charged positive ions $(n^+(\vec{r},t), \vec{J}_+(\vec{r},t,\vec{E}))$ and the electrons $(n^-(\vec{r},t), \vec{J}_-(\vec{r},t,\vec{E}))$ are retained.

The charged particles rarely encounter one another in binary collisions in the gas, as compared with their collisions with neutrals. However, they do interact through the macroscopic fields set up by aggregations of charges. These interactions, as well as the diffusive flow of the particles in the background gas, are accounted for in the expression for the current densities and in Poisson's equation relating the local electric field to the charge density.

$$\vec{J}_\pm(\vec{r},t,\vec{E}) = n^\pm \mu^\pm \vec{E} - D^\pm \nabla n^\pm \tag{2}$$

$$\nabla \cdot E = \frac{e(n^+ - n^-)}{\epsilon_o} \tag{3}$$

where $\mu^{\pm}$ are the mobilities of the charged particles (μ^- being a negative number); $D^{\pm}$ are the ordinary diffusion coefficients; e is the electronic charge, and ϵ_o is the permittivity of free space.

In this development it is assumed that there is no constant magnetic field present and that the interaction with self-generated $\vec{B}$ fields is of second order. Hence, the mobility and diffusion constants will be scalar constants.

The next step used in the classical method of analyzing the discharge behavior is to make the steady-state assumptions

(a) Congruence, $\vec{J}_+ = \vec{J}_-$, and

(b) Proportionality, $\nabla n^+/n^+ = \nabla n^-/n^-$.

The result of these two approximations is to make Eqs. 2 solvable directly by elimination of $\vec{E}$ between them. The result is the ambipolar-diffusion equation, the solution of which is well known. But with striations moving in the plasma, neither of these assumptions is correct for all spacial positions at all times. The proportionality assumption is particularly shaky unless the plasma is very tenuous, in which case both types of charge carrier satisfy the free diffusion equation; or unless the plasma is very dense, in which case the difference between n^+ and n^- is very small. Since we seek both the time and space variation of the variables involved, we shall avoid these assumptions and proceed as follows.

The equations resulting from the substitution of Eqs. 2 in Eqs. 1 are:

$$\frac{\partial n}{\partial t} = -\nabla \cdot (n^{\pm}\mu^{\pm}\vec{E}) + D^{\pm}\nabla^2 n^{\pm} + R_i^{\pm} - R_a^{\pm} \tag{4}$$

if $D^{\pm}$ are assumed to be constant, which is a fairly good approximation.

The functions $R_i^{\pm}$ and $R_a^{\pm}$ are the source terms for (4). The former represents the ionization rate per unit volume and the latter, the recombination rate per unit volume. To a good approximation, $R_i^{\pm} \gg R_a^{\pm}$ over all space and time. Therefore, $R_a^{\pm}$ will be neglected.

Another approximation is made by considering the ionization rate to be proportional to the electron concentration only. This is justified by the fact that the average energies of the positive ions are small compared with those of the electrons; and they do not cause ionizations upon collision with neutrals. Virtually all of the ionization is caused by electron collisions with neutrals. Therefore

$$R_i^{\pm} = \nu_i n^-, \tag{5}$$

where ν_i is the collision frequency for ionization per particle. Expanding (4) and grouping terms, we obtain

$$\frac{\partial n^-}{\partial t} - \nabla^2(D^- n^-) + \nabla \cdot (n^- \mu^- \vec{E}) - \nu_i n^- = 0 \tag{6}$$

$$\frac{\partial n^+}{\partial t} - \nabla^2(D^+n^+) + \nabla \cdot (n^+\mu^+\vec{E}) - \nu_i n^- = 0. \qquad (7)$$

Equations 6 and 7, together with Eqs. 3, comprise a set of coupled, nonlinear, partial differential equations that can, in principle, be solved for the functions of interest, $n^{\pm}(\vec{r}, t)$ and $\vec{E}$.

R. S. Cooper

References

1. W. Pupp, Oszillographische Sondenmessungen an laufenden schichten der positiven Saule von Edelgasen, Physik. Z. 36, 61 (1935).

2. I. Langmuir and L. Tonks, Oscillations in ionized gases, Phys. Rev. 33, 195 (1929).

3. W. P. Allis, Notes on Plasma Dynamics, Summer Session Class Notes, M.I.T., 1959, pp. E1-E3.

4. A. B. Stewart, Oscillating glow discharge plasma, J. Appl. Phys. 27, 911 (1956).

C. THERMIONIC PROPERTIES OF MONOCRYSTALLINE TANTALUM

The thermionic characteristics of the (110) face of monocrystalline tantalum exposed to a cesium vapor are being examined. Previous experiments with tantalum and other refractory metals clearly indicate the general properties: electron emission is increased, and ions are emitted from the hot surface.[1,2]

A single crystal is used, partly because the properties are known to depend on crystallographic direction and the (110) face is the best adsorber of cesium since it has the highest work function (4.75 volts) of all tantalum surfaces, and partly because the details of the surface are more accurately known than for a polycrystalline surface.

1. Apparatus

A diode has been constructed and is illustrated schematically in Fig. XII-15. The envelope is glass. The emitter and collector are identical, except that the emitter has a platinum-rhodium thermocouple in the back of it and an electron bombardment heater. Each crystal is a disc, 0.25 inch in diameter; the spacing (between 5 and 30 mils) depends on the temperature of the emitter. There is a guard ring whose potential can be varied to prevent current passing through the space from the supports of the diode electrodes. Platinization on the wall of the tube that is connected to the guard ring prevents excessive leakage of current along the walls between emitter and collector leads.

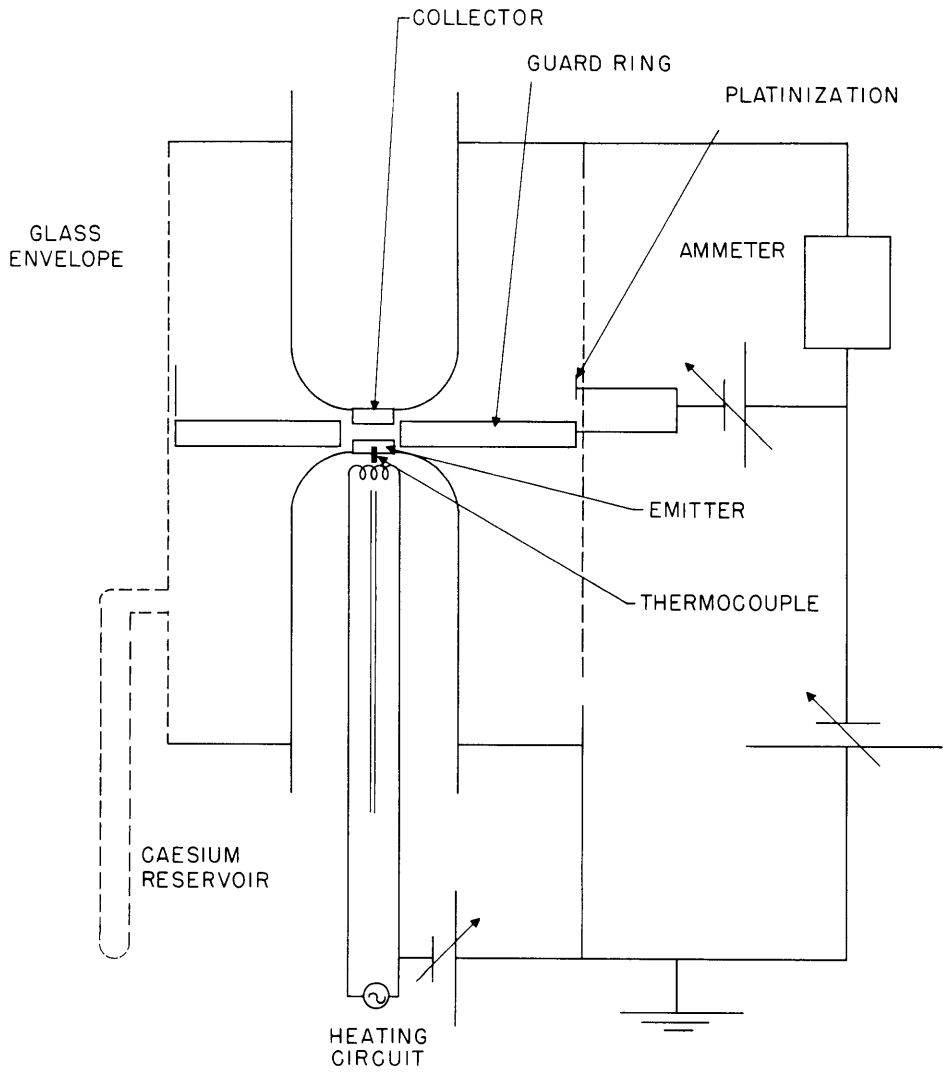

Fig. XII-15. Schematic arrangement of experimental apparatus.

Preliminary experiments were run with an x-y recorder with a cesium reservoir temperature of 300°K. For different temperatures of the emitter, voltage-current curves for the diode were made. A selection of these is shown in Fig. XII-16. The leakage current is an appreciable fraction of the diode current at these low cesium-bath temperatures. Marked on each curve are points considered to correspond to the value of the saturated electron current from the emitter. After allowance was made for the leakage current, the effective work function, which is the value of ϕ_e to satisfy the Richardson-Dushman equation

$$i = 120\,T^2 \exp\left(-\frac{\phi_e e}{kT}\right),$$

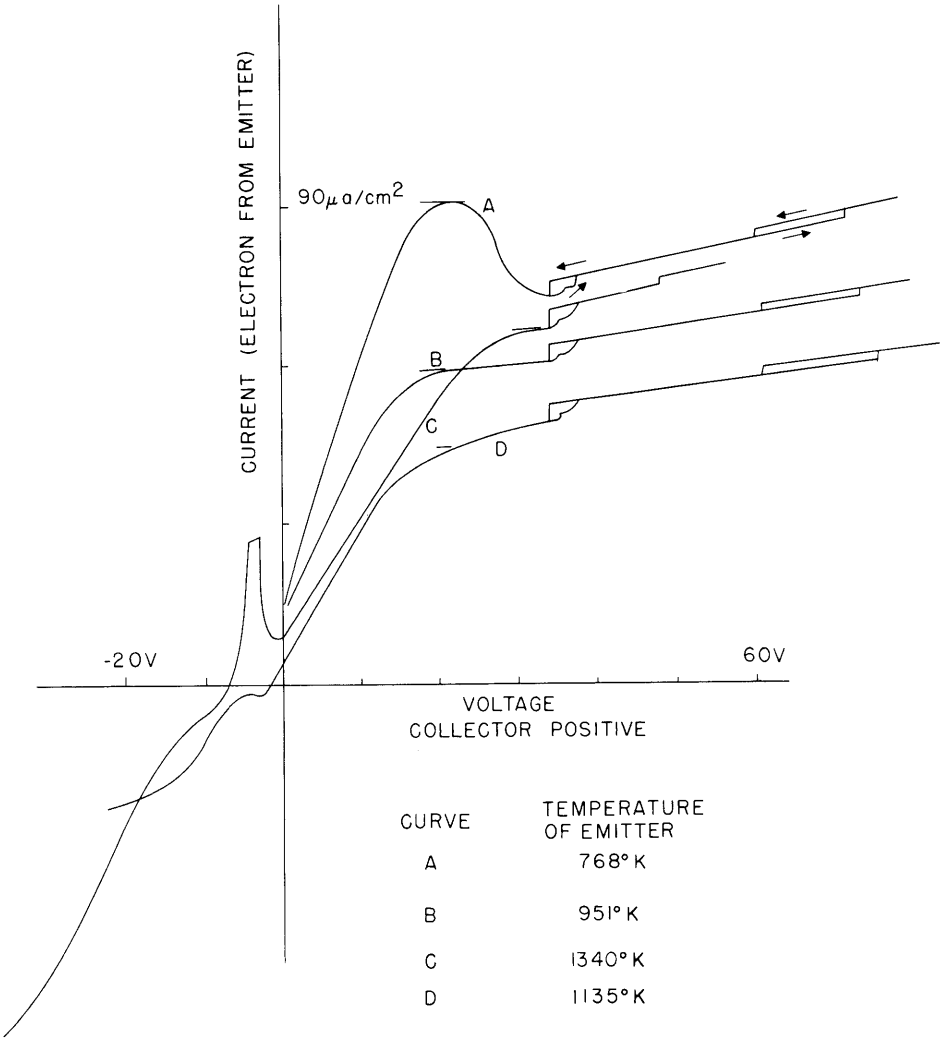

Fig. XII-16. Voltage-current curves at a number of emitter temperatures. (Horizontal-line marks indicate saturation current.)

was computed for each pair of electron current and temperature. The variation of the work function with emitter temperature is shown in Fig. XII-17 as circles, and is compared with results for polycrystalline tantalum (solid line). The low work function of the coated surface is that which was expected. Also marked is the approximate temperature at which significant ion current begins to flow, and at which the work function should be ~3.9 volts, if the Saha-Langmuir equation is correct. Figure XII-18 shows the variation of the "ion current" with temperature when the voltage across the tube is 10 volts.

There are several anomalies:

(a) hysteresis effects around 30 volts and 65 volts;

(b) rise in emission current at 50 volts;

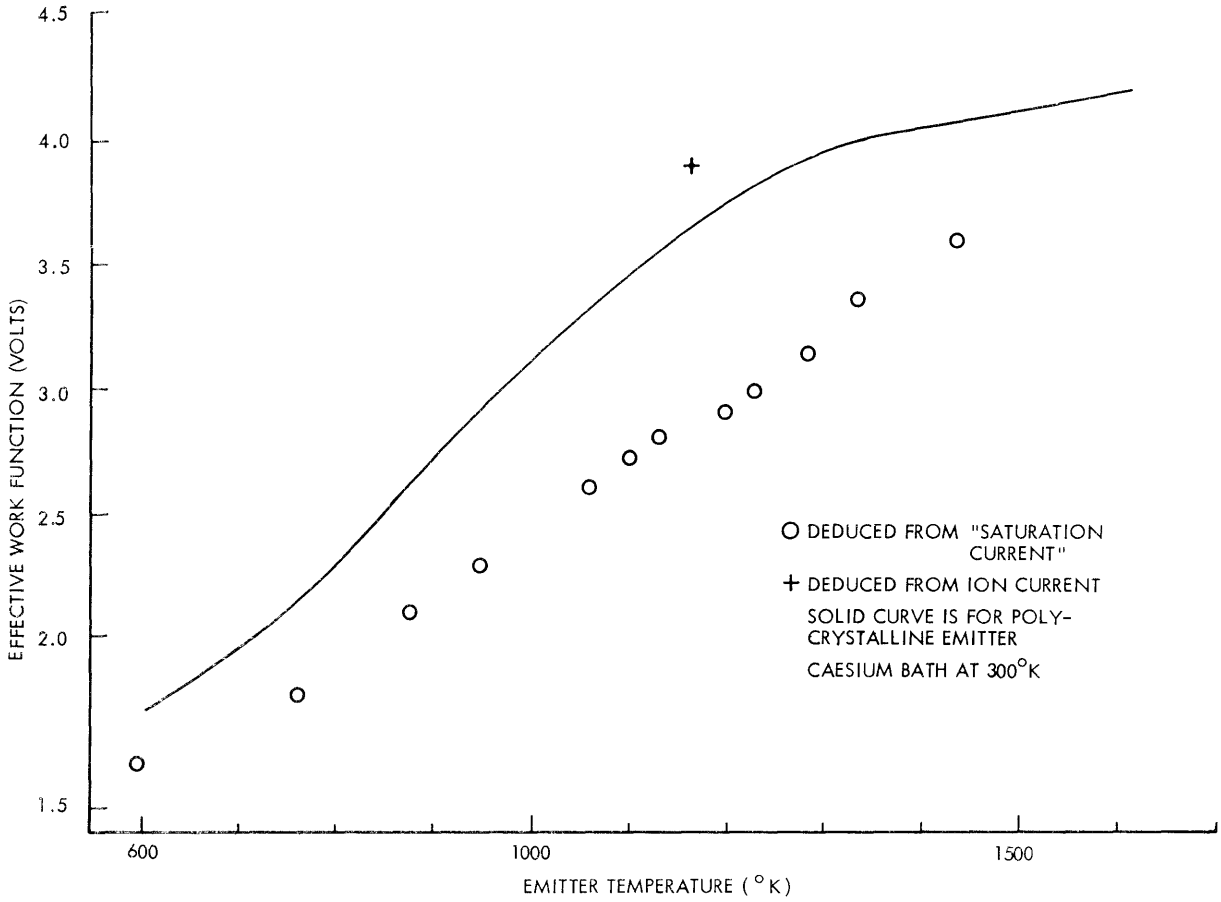

Fig. XII-17. Effective work function vs emitter temperature with the cesium bath at 300°K.

(c) negative resistance at small voltages in the power-producing region; and

(d) disparity of values of effective work function which are calculated from the ion current and electron emission, and the fact that at higher emitter temperatures the ion current is even in excess of the random atom current in the cesium vapor.

Possible explanations of the phenomena could be formulated by taking into account:

(a) Photoemission from the collector. It has a very low work function and the radiation falling on it is considerable.

(b) Oscillations may be taking place at higher emitter temperatures.

(c) Radiation from the emitter may well heat up the collector sufficiently for the thermal electron emission from it to interfere with the potential distribution.

(d) The Saha-Langmuir equation may not correctly describe ion emission from a surface with adsorbed atoms, despite the experiments of Taylor and Langmuir,[2] whose work alone suggests that it does.

Further experiments are being conducted at higher cesium pressures and with

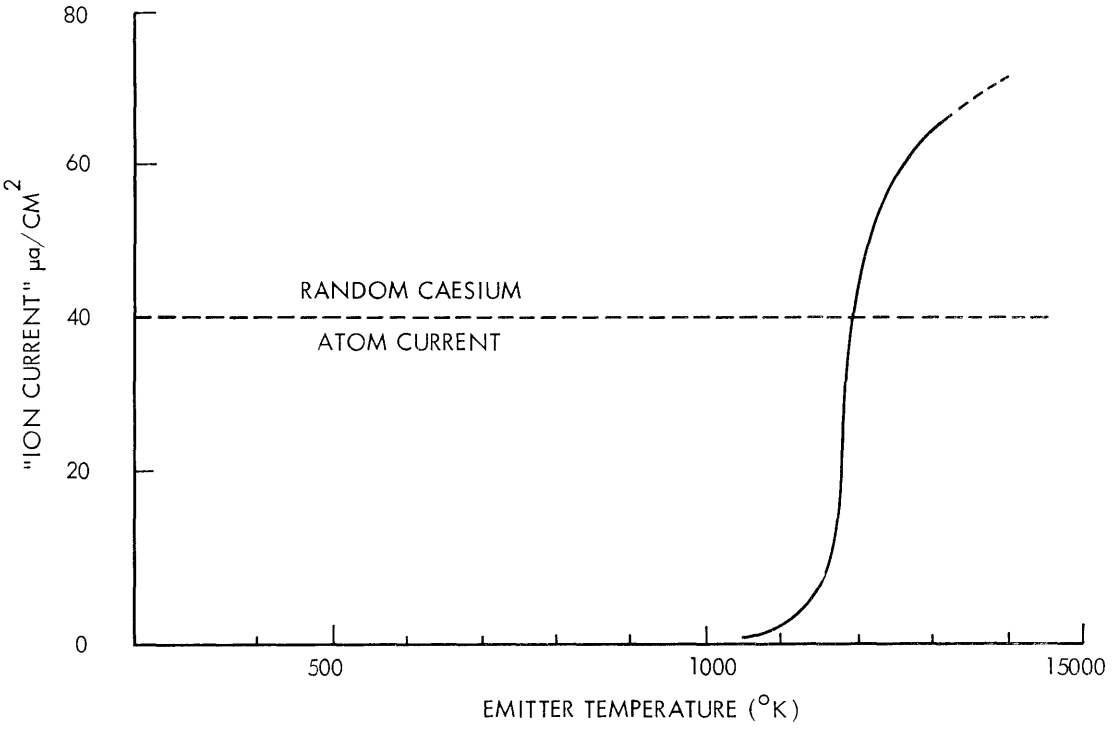

Fig. XII-18. "Ion current" with 10 volts across the diode vs emitter temperature.

modified apparatus to examine the validity of these explanations.

We are also trying to interpret the cesium film properties in terms of a lattice gas by using modifications of the standard methods[3] and trying to take account of the presence of ions on the surface.

W. T. Norris

References

1. S. Datz and E. H. Taylor, Ionization on platinum and tungsten surfaces. I. The alkali metals, J. Chem. Phys. 25, 389-394 (1956).

2. I. Langmuir and J. B. Taylor, Evaporation of atoms, ions, and electrons from cesium films on tungsten, Phys. Rev. 44, 423 (1933).

3. R. H. Fowler and E. A. Guggenheim, Statistical Thermodynamics (Cambridge University Press, London, 1952), pp. 437-438.

D. FUEL CELLS

Study of oxygen transport at oxygen electrodes continues. Electrolyte saturated with oxygen is made to flow past a totally submerged nonporous electrode of smooth platinum or silver. Findings are as follows:

(a) Oxygen electrodes totally submerged some distance in a stagnant electrolyte develop only a minute steady-state current. By circulating electrolyte containing dissolved oxygen past such a submerged electrode, the current is made to increase; thus it is indicated that operations are now controlled by mass transfer of oxygen. At substantially higher velocities, the attainable current density reaches a maximum, independently of flow velocity. The rate-controlling step is now no longer mass transfer, but instead is an adsorption process or a chemical reaction. On smooth platinum at 25°C, this "limiting electrochemical rate" was found to be sufficient to support a current density of 1 ma/cm^2 at 0.35 volt below the reversible oxygen potential for 20 per cent KOH saturated with oxygen at 1 atmosphere.

(b) When operating a submerged electrode and causing an electrolyte to flow past it at such velocities that mass transfer controls, the current developed at any given voltage increases with the concentration of the dissolved oxygen.

Curves of voltage versus current density are being obtained for various conditions of velocity, oxygen concentration, pH, temperature, and so forth.

Interpretation of the performance of a porous plate electrode in terms of these findings is under way. Calculations can be simplified by assuming that the micropores in such electrodes are cylindrical in shape, filled with electrolyte. Oxygen dissolves in the electrolyte-gas interface located somewhere within the pore, and this dissolved gas then diffuses down the pore to the pore walls. Concentration of oxygen in the electrolyte falls off rapidly, as a consequence, but rates of mass transport are fast enough, at first, so that sufficient oxygen reaches the wall to maintain the "limiting electrochemical rate." This would be 1 ma/cm^2 for a platinum system operating under the conditions outlined above. A point is soon reached where transport rates fall to a level at which current densities can no longer be maintained at this level. The narrower the pore, the shorter this distance. The bulk of the electrochemical action occurs within the short distance in which this "limiting rate" can be maintained, with little additional reaction occurring at greater distances into the pore. This distance, within which the bulk of the electrochemical action occurs, is called here the "active length" of the pore. Preliminary calculations show that for a pore 30 Å in diameter, with a limiting current density of 1 ma/cm^2 of pore wall, the active length would be $\sim 3 \times 10^{-5}$ cm, or 100 diameters. Other preliminary calculations show that, given the proper micro-macro pore structure, electrode configurations can be imagined for which electrodes should show current densities in excess of 1 amp/cm^2 of face area.

H. P. Meissner